International Journal of Solids and Structures 47 (2010) 71–80

Contents lists available at ScienceDirect

International Journal of Solids and Structures

journal homepage: www.elsevier.com/locate/ijsolstr

Analysis of cracked magnetoelectroelastic composites under time-harmonic loading

R. Rojas-Díaz [a], F. García-Sánchez [b,*], A. Sáez [a]

[a] Departamento de Mecánica de Medios Continuos, E.T.S. de Ingenieros, Universidad de Sevilla, Camino de los Descubrimientos s/n, 41092 Sevilla, Spain
[b] Departamento de Ingeniería Civil, de Materiales y Fabricación, E.T.S. de Ingenieros Industriales, Universidad de Málaga, Campus de El Ejido s/n, 29013 Málaga, Spain

ARTICLE INFO

Article history:
Received 3 March 2009
Received in revised form 11 May 2009
Available online 16 September 2009

Keywords:
Crack
Magnetoelectroelastic materials
Wave scattering
Dynamics
Boundary element method (BEM)

ABSTRACT

This paper presents a numerical model for the analysis of cracked magnetoelectroelastic materials subjected to in-plane mechanical, electric and magnetic dynamic time-harmonic loading. A traction boundary integral equation formulation is applied to solve the problem in combination with recently obtained time-harmonic Green's functions (Rojas-Diaz et al., 2008). The hypersingular boundary integral equations appearing in the formulation are first regularized via a simple change of variables that permits to isolate the singularities. Relevant fracture parameters, namely stress intensity factors, electric displacement intensity factor and magnetic induction intensity factor are directly evaluated as functions of the computed nodal opening displacements and the electric and magnetic potentials jumps across the crack faces. The method is checked by comparing numerical results against existing solutions for piezoelectric solids. Finally, numerical results for scattering of plane waves in a magnetoelectroelastic material by different crack configurations are presented for the first time. The obtained results are analyzed to evaluate the dependence of the fracture parameters on the coupled magnetoelectromechanical load, the crack geometry and the characteristics of the incident wave motion.

1. Introduction

Magnetoelectroelastic composites that combine piezoelectric and piezomagnetic phases have drawn significant attention in recent years due their ability to convert energy among magnetic, electric and mechanical fields. This is the reason why they are finding increasing use in smart structures applications. Such magnetoelectromechanical coupling may be found as well in some single-phase materials where simultaneous magnetic and electric ordering coexist. However, the main advantage of such composites as compared to the single-phase materials is that the resulting electromagnetic coupling may be even a hundred times larger (Van Suchtelen, 1972; Nan, 1994; Eerenstein et al., 2006).

As the use of magnetoelectroelastic composites in engineering increases, fracture mechanics of this class of materials has become an emerging research front where a large effort is focused on understanding the failure mechanisms involved and, subsequently, on generalizing some of the tools previously developed for anisotropic or piezoelectric fracture analysis to the magnetoelectroelastic case. Significant contributions have been done by several authors for static fracture: works by Wang and Mai (2003, 2004, 2007), Gao et al. (2003a,b, 2004), Tian and Gabbert (2004, 2005) or Li and Kardomateas (2006) should be cited among others.

However, the analysis of dynamic fracture problems of magnetoelectroelastic materials is more limited so far, not to mention that the majority of such analysis deals with anti-plane fracture, using semi-analytical solution methods. Zhou and Wang used the Schmidt method to investigate the dynamic behavior of an interface crack in a magnetoelectroelastic composite under harmonic elastic anti-plane shear waves (Zhou and Wang, 2005), and further extended this technique to analyze the cases of two collinear symmetric interface cracks between two dissimilar magnetoelectroelastic half planes (Zhou et al., 2005), two parallel symmetry cracks (Zhou and Wang, 2006), two parallel symmetry interface cracks (Zhou et al., 2006), two collinear interface cracks between two dissimilar functionally graded piezoelectric/piezomagnetic material strips (Zhang et al., 2007) and an interface crack between two dissimilar functionally graded piezoelectric/piezomagnetic material half infinite planes subjected to harmonic anti-plane shear stress waves (Zhou and Wang, 2008). Hu and Li (2005) derived the analytical solution for an anti-plane Griffith moving crack inside an infinite magnetoelectroelastic medium under the assumption of permeable crack faces and later extended this study to the case of an anti-plane Griffith crack moving at the interface between two dissimilar magnetoelectroelastic media (Hu et al., 2006). Li (2005) investigated the transient response of a magnetoelectroelastic medium containing a crack along the poling direction subjected to antiplane mechanical and inplane electric and magnetic impacts. Feng and Su (2006)) analyzed the dynamic anti-plane problem for a functionally graded magnetoelectroelastic

* Corresponding author.
E-mail addresses: rrojasdiaz@us.es (R. Rojas-Díaz), fgsanchez@uma.es (F. García-Sánchez), andres@us.es (A. Sáez).

0020-7683/$ - see front matter © 2009 Elsevier Ltd. All rights reserved.
doi:10.1016/j.ijsolstr.2009.09.011

strip containing an internal crack perpendicular to the boundary, under both magnetoelectrically impermeable or permeable boundary conditions on the crack faces. Zhong and Li (2006) studied the dynamic problem of an anti-plane shear crack of finite length moving with a constant velocity along the interface of two dissimilar magnetoelectroelastic materials. Feng et al. (2007) analyzed the dynamic behavior induced by a penny-shaped crack in a magneto-electroelastic layer subjected to prescribed stress or prescribed displacement at the layer surfaces for both impermeable and permeable cracks. Su et al. (2007) studied the problem of an arbitrary number of interface cracks between dissimilar magnetoelectroelastic strips under out-of-plane mechanical and in-plane magneto-electrical impacts. Yong and Zhou (2007) considered the transient anti-plane problem of a magnetoelectroelastic strip containing a crack vertical to the boundary. Liang (2008) derived the solution for the dynamic behavior of two parallel symmetric cracks in functionally graded piezoelectric/piezomagnetic materials subjected to harmonic antiplane shear waves. Feng and Pan (2008) investigated the anti-plane problem for an interfacial crack between two dissimilar magnetoelectroelastic plates subjected to anti-plane mechanical and in-plane magneto-electrical impact loadings under different combinations of magnetically and electrically permeable/impermeable surface conditions on the crack. More recently, Sladek et al. (2008) presented a meshless method based on the local Petrov-Galerkin approach for stationary and transient dynamic crack analysis in two-dimensional and three-dimensional axisymmetric magnetoelectroelastic solids with continuously varying material properties.

In this paper, a dual BEM formulation is presented for the analysis of cracked fully anisotropic magnetoelectroelastic composite solids under in-plane mechanical, electric and magnetic dynamic time-harmonic loading. The approach presented herein is a generalization to magnetoelectroelastic materials of our previous works for dynamic fracture of anisotropic and piezoelectric media (García-Sánchez et al., 2006; Sáez et al., 2006). The time-harmonic fundamental solution derived by Rojas-Diaz et al. (2008) using the Radon transform is split into singular plus regular parts. The singular part is independent of the frequency and it coincides with the static fundamental solution. In this way, the treatment of all the singularities arising in the BEM formulation follows the same regularization scheme presented by García-Sánchez et al. (2007) for statics, so that in order to solve the dynamic problem only regular terms need to be added to the static BEM. Quadratic elements are introduced for the boundary discretization, with straight quarter-point elements at the crack tips to adequately model the behavior of the field variables around the crack tips. Stress intensity, electric displacement and magnetic induction intensity factors are directly extrapolated from the computed nodal values at the quarter-point elements. The formulation is validated by considering wave scattering by a Griffith crack in a degenerate quasi-piezoelectric solid, since for this problem analytical solutions are available (Shindo and Ozawa, 1990). Some other numerical results are presented for a $BaTiO_3$–$CoFe_2O_4$ composite material to illustrate the accuracy and possibilities of the present approach.

2. Numerical modeling of dynamic fracture by BEM

The behavior of stationary cracks subjected to dynamic time-harmonic loading in plane magnetoelectroelastic solids will be addressed by a dual BEM formulation (Hong and Chen, 1988; Portela et al., 1992). The approach summarized within this section is an extension to the magnetoelectroelastic case of our previous work for anisotropic and piezoelectric crack problems (García-Sánchez et al., 2006; Sáez et al., 2006).

2.1. Constitutive equations

Consider a homogeneous, linear and fully anisotropic magneto-electroelastic plane solid. Its constitutive relations may be written as (Soh and Liu, 2005)

$$\sigma_{ij} = C_{ijkl}\varepsilon_{kl} - e_{lij}E_l - h_{lij}H_l \tag{1}$$

$$D_i = e_{ikl}\varepsilon_{kl} + \epsilon_{il}E_l + \beta_{il}H_l \tag{2}$$

$$B_i = h_{ikl}\varepsilon_{kl} + \beta_{il}E_l + \gamma_{il}H_l \tag{3}$$

where σ_{ij}, D_i and B_i are the mechanical stresses, the electric displacements and the magnetic inductions; C_{ijkl}, ϵ_{il} and γ_{il} are the elastic stiffness tensor, the dielectric permitivities and the magnetic permeabilities; e_{lij}, h_{lij} and β_{il} are the piezoelectric, piezomagnetic and magnetoelectric coupling coefficients; and ε_{ij}, E_i and H_i are, respectively, the mechanical strains, the electric field and the magnetic field which are related with the elastic displacements, u_i, the electric potential, ϕ and the magnetic potential, φ, by the following expressions.

$$\varepsilon_{ij} = \frac{1}{2}(u_{i,j} + u_{j,i}) \tag{4}$$

$$E_i = -\phi_{,i} \tag{5}$$

$$H_i = -\varphi_{,i} \tag{6}$$

Eqs. (1)–(3) can be written in a more compact form as

$$\sigma_{iJ} = C_{iJKl}u_{K,l} \tag{7}$$

when the extended notation is considered, in such a way that the displacement vector is extended with the electric potential and the magnetic potential as

$$u_I = \begin{cases} u_i & I = 1,2 \\ \phi & I = 4 \\ \varphi & I = 5 \end{cases} \tag{8}$$

and the stress tensor is extended with the electric displacements and the magnetic inductions as

$$\sigma_{iJ} = \begin{cases} \sigma_{ij} & J = 1,2 \\ D_i & J = 4 \\ B_i & J = 5 \end{cases} \tag{9}$$

whilst the elasticity tensor is extended as

$$C_{iJKl} = \begin{cases} C_{ijkl} & J,K = 1,2 \\ e_{lij} & J = 1,2;\ K = 4 \\ h_{lij} & J = 1,2;\ K = 5 \\ e_{ikl} & J = 4;\ K = 1,2 \\ -\epsilon_{il} & J,K = 4 \\ -\beta_{il} & J = 4;\ K = 5 \\ h_{ikl} & J = 5;\ K = 1,2 \\ -\beta_{il} & J = 5;\ K = 4 \\ -\gamma_{il} & J,K = 5 \end{cases} \tag{10}$$

so that the lowercase (elastic) and uppercase (extended) subscripts adopt values 1, 2 and 1, 2 (mechanical), 4 (electric), 5 (magnetic), respectively.

2.2. Governing equations

The dynamic equilibrium equations for an elastic medium under time-harmonic loading are given by

$$\sigma_{ij,j}(\boldsymbol{x},\omega)+\rho\omega^2 u_i(\boldsymbol{x},\omega)=-b_i(\boldsymbol{x},\omega) \tag{11}$$

where ω is the frequency of excitation, ρ is the mass density of the material and $b_i(\boldsymbol{x},\omega)$ are the body forces.

Taking into account that the characteristic frequencies in pure mechanical and pure electromagnetic problems are very different, say by 3 orders of magnitude, typical time variations for the mechanical field can be considered as quasi-static for the electric and magnetic fields (Parton and Kudryavtsev, 1988), so that the Maxwell equations can be written as

$$D_{j,j}(\boldsymbol{x},\omega)=f_D(\boldsymbol{x},\omega) \tag{12}$$

$$B_{j,j}(\boldsymbol{x},\omega)=f_B(\boldsymbol{x},\omega) \tag{13}$$

where $f_D(\boldsymbol{x},\omega)$ is the electric charge density and $f_B(\boldsymbol{x},\omega)$ is the magnetic induction source.

Eqs. (11)–(13) constitute the set of governing equations for the dynamic time-harmonic problem of MEE materials. They can be rewritten in a more compact form by using the extended notation described above, to yield

$$C_{iJKl}u_{K,il}(\boldsymbol{x},\omega)+\rho\omega^2\delta^*_{JK}u_K(\boldsymbol{x},\omega)=-F_J(\boldsymbol{x},\omega) \tag{14}$$

where δ^*_{JK} is the generalized Kronecker delta defined as

$$\delta^*_{JK}=\begin{cases}\delta_{jk} & J,K=1,2\\ 0 & \text{otherwise}\end{cases}, \tag{15}$$

and F_J is the extended body forces vector

$$F^*_J=\begin{cases}b_j & J=1,2\\ -f_D & J=4\\ -f_B & J=5\end{cases}. \tag{16}$$

2.3. Green's functions

Green's functions are defined as the response of an infinite homogeneous linear magnetoelectroelastic plane solid due to the application of a time-harmonic point force (in the extended sense). In this work we consider the Green's functions derived by (Rojas-Diaz et al., 2008) using the Radon transform technique. Green's functions are thus obtained in the form of line integrals over a unit circle ($|\eta|=1$) as the superposition of singular terms, that are frequency independent, plus regular terms

$$u^*_{IJ}(\boldsymbol{x},\xi,\omega)=u^{*S}_{IJ}(\boldsymbol{x},\xi)+u^{*R}_{IJ}(\boldsymbol{x},\xi,\omega) \tag{17}$$

where ω is the frequency of excitation, ξ is the point where the load is applied, $\boldsymbol{x}$ is the point where the displacements are obtained and

$$u^{*S}_{IJ}(\boldsymbol{x},\xi)=-\frac{1}{4\pi^2}\int_{|\boldsymbol{\eta}|=1}\frac{\varepsilon^q_{IJ}}{\rho c_q^2 E^q_{pp}}\log|\boldsymbol{\eta}\cdot\boldsymbol{r}|dL(\boldsymbol{\eta}) -\frac{1}{4\pi^2}\int_{|\boldsymbol{\eta}|=1}\Lambda_{IJ}\log|\boldsymbol{\eta}\cdot\boldsymbol{r}|dL(\boldsymbol{\eta}) \tag{18}$$

$$u^{*R}_{IJ}(\boldsymbol{x},\xi,\omega)=\frac{1}{16\pi^2}\int_{|\boldsymbol{\eta}|=1}\frac{\varepsilon^q_{IJ}}{\rho c_q^2 E^q_{yy}}\Phi^R(k_q,|\boldsymbol{\eta}\cdot\boldsymbol{r}|)dL(\boldsymbol{\eta}) \tag{19}$$

where $\boldsymbol{r}=\xi-\boldsymbol{x}$ and ε^q_{IJ} and Λ_{IJ} are given by

$$\varepsilon^q_{IJ}=\begin{cases}E^q_{ij} & I,J=1,2\\ \alpha^I_l E^q_{lj} & I=4,5;\quad J=1,2\\ \alpha^I_l\alpha^J_m E^q_{lm} & I,J=4,5\end{cases} \tag{20}$$

$$\Lambda_{IJ}=\frac{\Gamma_{IJ}(\delta_{4I}\delta_{5J}+\delta_{5I}\delta_{4J})-\frac{\Gamma_{44}\Gamma_{55}}{\Gamma_{IJ}}(\delta_{4I}\delta_{4J}+\delta_{5I}\delta_{5J})}{\Gamma_{45}\Gamma_{54}-\Gamma_{44}\Gamma_{55}}, \tag{21}$$

and E^q_{pk} is defined as

$$E^q_{pk}=adj\{Z_{pk}-\rho c_q^2\delta_{pk}\} \tag{22}$$

with $k_q=\omega/c_q$ being the wave numbers and c_q being the phase velocities, obtained as the roots of the following characteristic equation

$$det(Z_{pk}-\rho c_q^2\delta_{pk})=0 \tag{23}$$

with

$$Z_{pk}=\Gamma_{pk}+\alpha^4_k\Gamma_{p4}+\alpha^5_k\Gamma_{p5}, \tag{24}$$

and Γ_{PK} being the generalized Christoffel tensor given by

$$\Gamma_{PK}=C_{mPKl}\eta_m\eta_l \tag{25}$$

and

$$\alpha^4_k=\frac{\Gamma_{4k}\Gamma_{55}-\Gamma_{45}\Gamma_{5k}}{\Gamma_{45}\Gamma_{54}-\Gamma_{44}\Gamma_{55}}, \tag{26}$$

$$\alpha^5_k=\frac{\Gamma_{44}\Gamma_{5k}-\Gamma_{4k}\Gamma_{54}}{\Gamma_{45}\Gamma_{54}-\Gamma_{44}\Gamma_{55}}. \tag{27}$$

The function Φ^R considered in Eq. (19) is given by

$$\Phi^R(k_q,|\boldsymbol{\eta}\cdot\boldsymbol{r}|)=\Phi(k_q|\boldsymbol{\eta}\cdot\boldsymbol{r}|)+2\log(|\boldsymbol{\eta}\cdot\boldsymbol{r}|) \tag{28}$$

where

$$\Phi(\zeta)=i\pi e^{i\zeta}-2[\cos(\zeta)ci(\zeta)+\sin(\zeta)si(\zeta)] \tag{29}$$

and ci and si are, respectively, the cosine integral and the sine integral defined by

$$ci(\zeta)=-\int_\zeta^\infty\frac{\cos z}{z}dz;\quad si(\zeta)=-\int_\zeta^\infty\frac{\sin z}{z}dz \tag{30}$$

The corresponding traction Green's functions p^*_{IJ} may be easily derived by substitution of u^*_{IJ} into the generalized Hooke's law to yield

$$p^*_{IJ}=n_rC_{rIMl}U_{MJ,l} \tag{31}$$

where n_r are the components of the external unit normal vector to the boundary at the observation point $\boldsymbol{x}$.

2.4. Dual BEM for time-harmonic problems

The dual BEM is based on the use of two independent boundary integral equations (BIE) to overcome the mathematical degeneration arising from the coincidence of the two crack surfaces in fracture applications: the displacements BIE and the tractions BIE. Consider a plane magnetoelectroelastic cracked solid Ω with boundary Γ, so that $\Gamma=\Gamma_C\cup\Gamma_{crack}$, where $\Gamma_{crack}=\Gamma_+\cup\Gamma_-$ are the two geometrically coincident crack surfaces and Γ_C denotes the crack-free boundary. The displacements at a point ξ of the domain Ω, when it is subjected to time-harmonic loading in the absence of body forces, are related to the displacements and the tractions at the boundary Γ through the following displacement BIE

$$c_{IJ}(\xi)u_J(\xi,\omega)+\int_\Gamma p^*_{IJ}(\boldsymbol{x},\xi,\omega)u_J(\boldsymbol{x},\omega)d\Gamma(\boldsymbol{x}) =\int_\Gamma u^*_{IJ}(\boldsymbol{x},\xi,\omega)p_J(\boldsymbol{x},\omega)d\Gamma(\boldsymbol{x}) \tag{32}$$

where the extended notation has been used. u^*_{IJ} and p^*_{IJ} denote the fundamental solution or Green's functions displacements and tractions at boundary point $\boldsymbol{x}$ due to a unit harmonic load placed at point ξ (Rojas-Diaz et al., 2008), with the expressions summarized in the previous section; and $c_{IJ}(\xi)$ results from the Cauchy principal value integration of the singular p^*_{IJ} kernels and thus depends on the geometry variation at the point ξ. The tractions BIE follows from differentiation of Eq. (32) with respect to ξ_k and application of Hooke's law, to yield

$$c_{IJ}(\xi)p_J(\xi,\omega) + N_q \int_\Gamma s^*_{qIJ}(\boldsymbol{x},\xi,\omega)u_J(\boldsymbol{x},\omega)d\Gamma(\boldsymbol{x}) = N_q \int_\Gamma d^*_{qIJ}(\boldsymbol{x},\xi,\omega)p_J(\boldsymbol{x},\omega)d\Gamma(\boldsymbol{x}) \tag{33}$$

where $q = 1,2$ and N_q denote the components of the outward unit normal to the boundary at the collocation point ξ and s^*_{qIJ} and d^*_{qIJ} are defined by

$$d^*_{qIJ} = C_{qIMl}\ u^*_{MJ,l} \tag{34}$$

$$s^*_{qIJ} = C_{qIMl}\ p^*_{MJ,l} \tag{35}$$

The fundamental solution kernels in Eqs. (32) and (33) show a weak singularity of order log(r) when $r = |\boldsymbol{r}| = |\xi - \boldsymbol{x}| \to 0$ for u^*_{IJ}, a strong singularity of order $1/r$ for p^*_{IJ} and d^*_{qIJ}, and a hypersingular behavior of the type $1/r^2$ for s^*_{qIJ}, so that integrals of s^*_{qIJ} in (33) are to be understood in a Hadamard principal value sense and a C^1 continuity of the displacements is required. This is achieved by the use of discontinuous elements when considering the traction BIE, as in (García-Sánchez et al., 2007). Provided that the singular part of the time-harmonic fundamental solution coincides with the fundamental solution for the static problem (i.e., the regular part of the solution vanishes as $\omega \to 0$), the treatment of all these singularities follows our previous work on regularization for statics (García-Sánchez et al., 2005, 2007). Furthermore, in this paper we consider and implement the explicit expressions for the 2D static magnetoelectroelastic Green's functions previously derived by Jiang and Pan (2004) (see (Rojas-Diaz et al., 2008) for details), which are given in Appendix A. Once the singular integrals associated to the static part of the solution have been properly addressed, only the regular frequency dependent terms have to be added to the static BEM formulation in order to solve the dynamic problem. As for piezoelectricity (Sáez et al., 2006), computation of the integrals involving the regular part of the fundamental solution imply a double numerical integration: first along the unit circumference ($|\boldsymbol{\eta}| = 1$) and then over the boundary element. In the case of the s^{*R}-kernels, the integration is done numerically with a logarithmic quadrature that accounts for the weak singularity shown by the tractions derivatives. Details about the integration of strongly singular and hypersingular integrals can be found in Appendix B.

2.5. Modeling fracture problems

In the dual BEM, the displacement BIE (32) is applied onto the crack-free boundary Γ_C and one of the crack surfaces, say Γ_-, whilst the traction BIE (33) is applied onto the other crack surface Γ_+ to yield a system of equations to obtain the extended displacements and tractions on the boundary Γ. Alternatively, if the cracks faces are free of mechanical tractions and electric and magnetic impermeable boundary conditions are considered on the crack faces ($\Delta p_J = p_J^+ + p_J^- = 0$), it will suffice to apply the displacement BIE on Γ_C

$$c_{IJ}u_J + \int_{\Gamma_c} p^*_{IJ}u_J d\Gamma + \int_{\Gamma_+} p^*_{IJ}\Delta u_J d\Gamma = \int_{\Gamma_c} u^*_{IJ}p_J d\Gamma \tag{36}$$

and the traction BIE on one of the crack surfaces, say Γ_+, to obtain a complete set of equations with the unknowns being the extended displacements and tractions on Γ_C and the extended crack opening displacements (ECOD: $\Delta u_J = u_J^+ - u_J^-$) on Γ_{crack}

$$p_J + N_q \int_{\Gamma_c} s^*_{qIJ}u_J d\Gamma + N_q \int_{\Gamma_+} s^*_{qIJ}\Delta u_J d\Gamma = N_q \int_{\Gamma_c} d^*_{rIJ}p_J d\Gamma \tag{37}$$

where the free term has been set to 1 because of the additional singularity arising from the coincidence of the two crack surfaces. This is the approach implemented in this paper since the ECOD are the relevant magnitudes to obtain the fracture parameters.

When dealing with fracture applications two key issues have to be addressed, namely:

1. Properly modeling the singular behavior of the field variables around the crack tip.
   Since the asymptotic behavior of the ECOD near the crack tip in a magnetoelectroelastic material shows the classical $\sqrt{\bar{r}}$ type of variation (Gao et al., 2003a,b; Wang and Mai, 2003), $\bar{r}$ being the radial polar coordinate with origin at the crack tip, the discontinuous straight quarter-point element (Fig. 1) previously presented by the authors for dynamic fracture applications in elastic anisotropic (García-Sánchez et al., 2006) and piezoelectric (Sáez et al., 2006) materials can be further extended to the magnetoelectroelastic case. Details of the meshing strategy, using quadratic elements, follow the same approach as for statics (García-Sánchez et al., 2007).
2. Evaluation of the fracture parameters.
   Stress (SIF: K_I and K_{II}), electrical displacement (EDIF: K_{IV}) and magnetic induction (MIIF: K_V) intensity factors can then be directly determined from the nodal values of the ECOD from

$$\begin{pmatrix} K_{II} \\ K_I \\ K_{IV} \\ K_V \end{pmatrix} = \sqrt{\frac{\pi}{8\hat{r}}}\quad \mathbf{H}^{-1} \begin{pmatrix} \Delta u_1 \\ \Delta u_2 \\ \Delta\phi \\ \Delta\varphi \end{pmatrix} \tag{38}$$

$\hat{r}$ being the distance between the crack tip and the nodal point where the ECOD are evaluated and

$$\mathbf{H} = \Re(\mathbf{M}) \tag{39}$$

where $\Re$ stands for the real part and $\mathbf{M}$ is defined in Appendix A. Other relevant fracture parameters follow from the field intensity factors, e.g., the total energy release rate G may be obtained from Tian and Rajapakse (2005)

$$G = \frac{1}{2}\mathbf{K}^T\mathbf{H}\mathbf{K} \tag{40}$$

where

$$\mathbf{K} = \begin{pmatrix} K_{II} \\ K_I \\ K_{IV} \\ K_V \end{pmatrix} \tag{41}$$

In the numerical examples shown in the next sections, Eq. (38) is particularized at the collocation node that is located the closest to

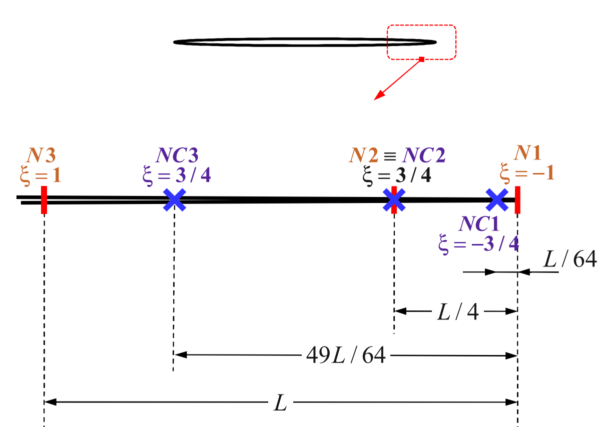

Fig. 1. Quadratic discontinuous quarter-point element.

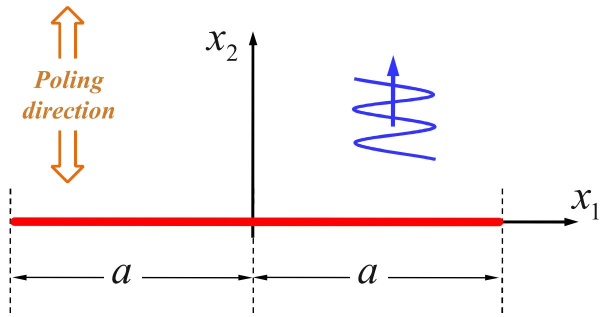

Fig. 2. Wave scattering by a Griffith crack in a PZT-6B piezoelectric solid.

Table 1
Material properties of $BaTiO_3$–$CoFe_2O_4$ (with $V_f = 0.5$).

C_{11} (GPa)	C_{12} (GPa)	C_{22} (GPa)	C_{66} (GPa)
226	125	216	44
e_{21} (C/m^2)	e_{22} (C/m^2)	e_{16} (C/m^2)	
−2.2	9.3	5.8	
h_{21} (N/Am)	h_{22} (N/Am)	h_{16} (N/Am)	
290.2	350	275	
ϵ_{11} (C^2/Nm^2)	ϵ_{22} (C^2/Nm^2)		
56.4×10^{-10}	63.5×10^{-10}		
β_{11} (Ns/VC)	β_{22} (Ns/VC)		
5.367×10^{-12}	2737.5×10^{-12}		
γ_{11} (Ns^2/C^2)	γ_{22} (Ns^2/C^2)		
297×10^{-6}	83.5×10^{-6}		

the crack tip, NC1 (Fig. 1: $\hat{r} = L/64$, L being the quarter-point element length), where the asymptotic behavior $\sqrt{\hat{r}}$ holds more precisely.

3. Validation of the formulation

To check the approach, the problem of scattering of time-harmonic longitudinal waves impinging normally onto a Griffith crack in a PZT-6B piezoelectric material is first considered. The crack is located perpendicular to the material poling axis (Fig. 2) and electrically impermeable conditions are assumed on the crack faces. Material properties and incident wave motion are described in the work by Shindo and Ozawa (1990), whose semi-analytical solution will be used for validation purposes.

The crack is meshed with 10 discontinuous quadratic elements, the ones at the tip being quarter-point elements. Fig. 3 shows, for the normalized mode-I SIF, the good agreement between the obtained results for a quasi-piezoelectric material and Shindo and Ozawa's solution.

4. Results and discussion

Next, for the sake of clarity, the contraction index technique introduced by (Voigt, 1910) will be used for the elastic stiffness tensor ($C_{ijkl} \to C_{\alpha\beta}$), the piezoelectric tensor ($e_{lij} \to e_{l\alpha}$) and the piezomagnetic tensor ($h_{lij} \to h_{l\alpha}$), in the following manner:

$$\alpha = \begin{cases} i \text{ if } i = j \\ 9 - (i + j) \text{ if } i \neq j \end{cases}; \quad \beta = \begin{cases} k \text{ if } k = l \\ 9 - (k + l) \text{ if } k \neq l \end{cases} \tag{42}$$

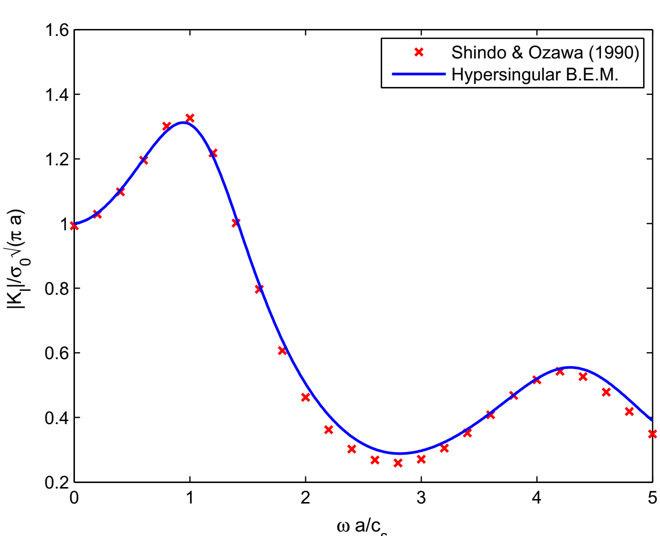

Fig. 3. Validation of the results: L-wave scattering by a Griffith crack in PZT-6B, K_I vs frequency.

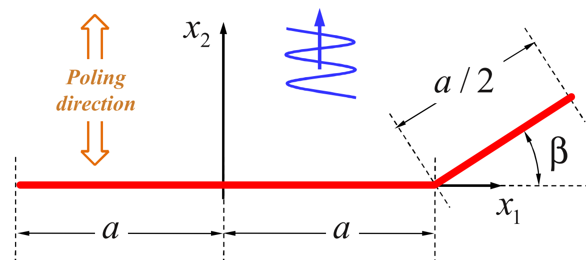

Fig. 4. Branched crack under impinging L-waves.

For the next examples a transversely isotropic $BaTiO_3$–$CoFe_2O_4$ magnetoelectroelastic composite with a volume fraction $V_f = 0.5$ will be considered. The material poling axis is aligned with the x_2-axis and its properties are listed in Table 1. Scattering of time-harmonic L-waves by a branched crack (Fig. 4) and a circular arch crack (Fig. 5) will be analyzed. The incident wave motion impinges along the x_2-axis, so that it is defined by the following extended displacement components

$$\begin{Bmatrix} u_1 \\ u_2 \\ \phi \\ \varphi \end{Bmatrix} = \begin{Bmatrix} 0 \\ u_0 \\ \phi_0 \\ \varphi_0 \end{Bmatrix} \exp[i\omega x_2/c_L] \tag{43}$$

where

$$c_L = \sqrt{\frac{1}{\rho}(C_{22} + \varkappa_1 e_{22} + \varkappa_2 h_{22})} \tag{44}$$

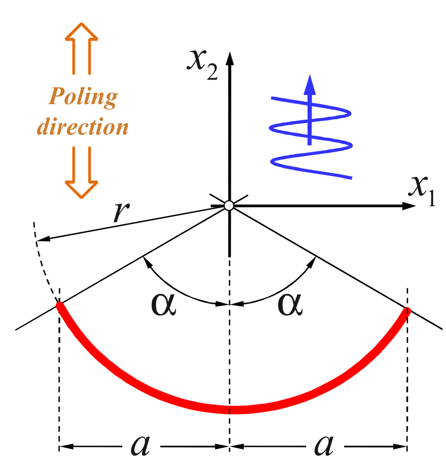

Fig. 5. Circular arch crack under impinging L-waves.

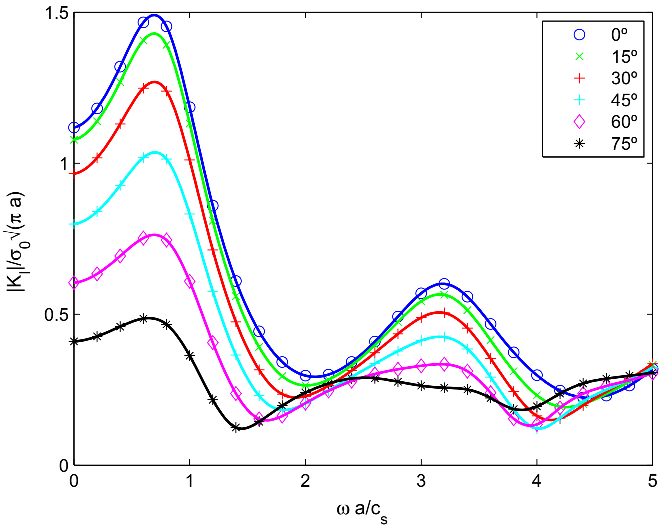

Fig. 6. L-wave scattering by a branched crack: K_I at branch tip vs. frequency for different branch angles β.

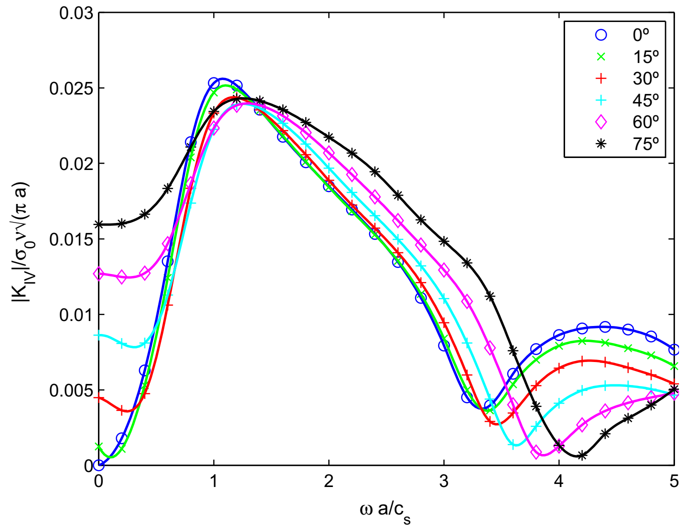

Fig. 8. L-wave scattering by a branched crack: K_{IV} at branch tip vs. frequency for different branch angles β.

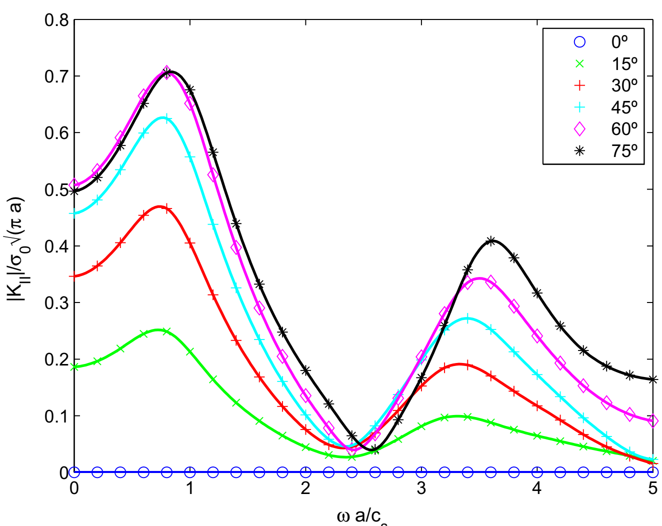

Fig. 7. L-wave scattering by a branched crack: K_{II} at branch tip vs. frequency for different branch angles β.

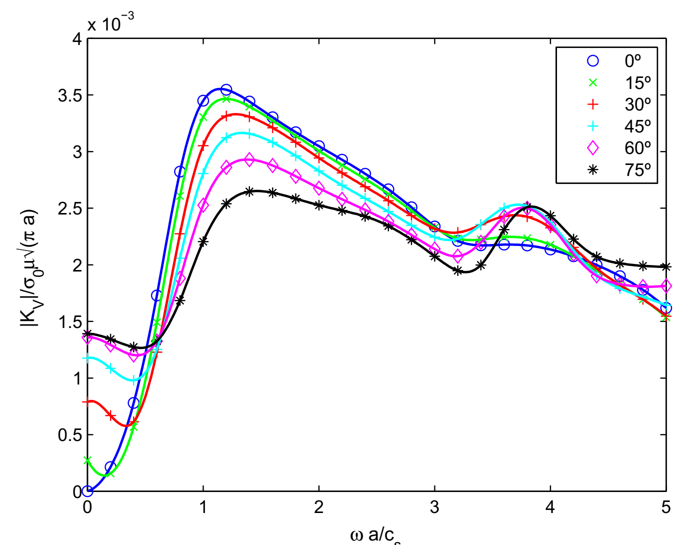

Fig. 9. L-wave scattering by a branched crack: K_V at branch tip vs. frequency for different branch angles β.

ρ being the mass density and

$$\varkappa_1 = \frac{\gamma_{22}e_{22} - \beta_{22}h_{22}}{\gamma_{22}\epsilon_{22} - \beta_{22}^2}; \quad \varkappa_2 = \frac{\epsilon_{22}h_{22} - \beta_{22}e_{22}}{\gamma_{22}\epsilon_{22} - \beta_{22}^2}. \tag{45}$$

The extended stresses associated to this wave motion follow from substitution of (43) into the constitutive law (7), so that the corresponding extended tractions at the crack surface with outward unit normal $\boldsymbol{n} = (n_1, n_2)$ will be given by

$$p_I = \begin{cases} p_1 = \sum_{j=1}^2 \sigma_{1j}n_j = \frac{C_{12}+e_{21}\varkappa_1+h_{21}\varkappa_2}{C_{22}+e_{22}\varkappa_1+h_{22}\varkappa_2} n_1\sigma_0 \exp[i\omega x_2/c_L] & I = 1 \\ p_2 = \sum_{j=1}^2 \sigma_{2j}n_j = n_2\sigma_0 \exp[i\omega x_2/c_L] & I = 2 \\ D_n = \sum_{j=1}^2 D_j n_j = 0 & I = 4 \\ B_n = \sum_{j=1}^2 B_j n_j = 0 & I = 5 \end{cases} \tag{46}$$

with

$$\sigma_0 = (C_{22} + e_{22}\varkappa_1 + h_{22}\varkappa_2)\frac{i\omega}{c_L}u_0 \tag{47}$$

where impermeable boundary conditions on the crack faces have been assumed so that

$$\phi_0 = \varkappa_1 u_0 \tag{48}$$

$$\varphi_0 = \varkappa_2 u_0. \tag{49}$$

4.1. Branched crack

Scattering of L-waves by a branched crack is first considered. The geometry of the problem is shown in Fig. 4. Results are obtained for several branch angles β. The main crack is meshed with 10 discontinuous quadratic elements, whilst five elements are used to mesh the crack branch. Elements at both crack tips are quarter-point elements. The normalized field intensity factors at the branch

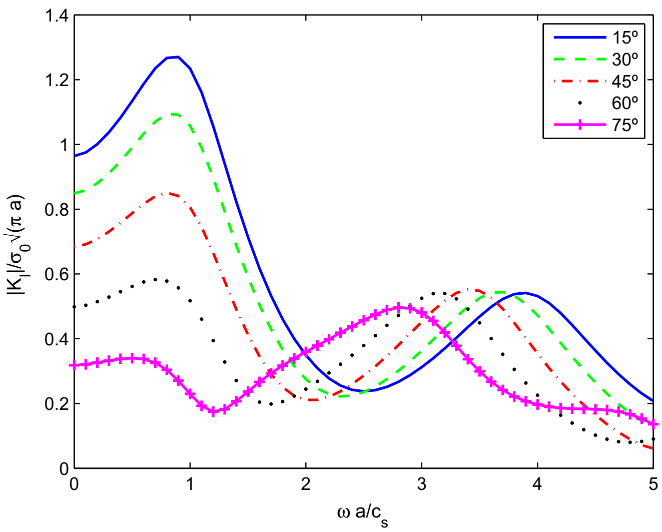

Fig. 10. L-wave scattering by a curved crack: K_I vs. frequency for different arch angles α.

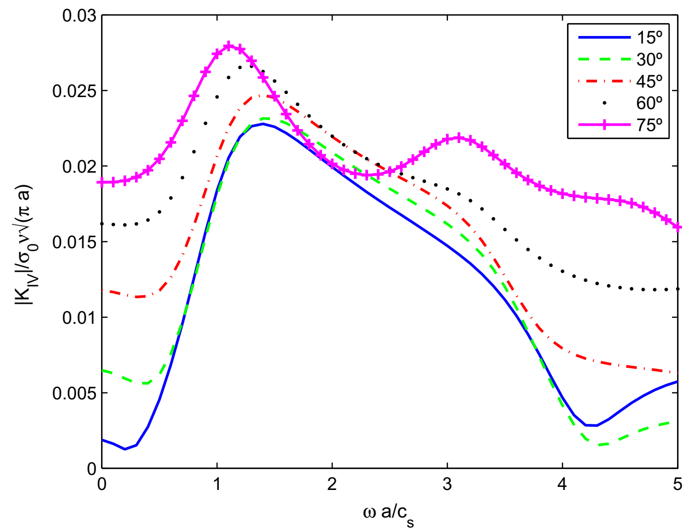

Fig. 12. L-wave scattering by a curved crack: K_{IV} vs. frequency for different arch angles α.

tip are plotted against the dimensionless frequency in Fig. 6 (K_I), Fig. 7 (K_{II}), Fig. 8 (K_{IV}) and Fig. 9 (K_V). The following quantities are introduced for normalization purposes

$$c_S = \sqrt{\frac{C_{66}}{\rho}}; \quad \nu = \frac{\epsilon_{22}}{e_{22}}; \quad \mu = \frac{\Gamma_{22}}{h_{22}} \tag{50}$$

The influence of the frequency of the incident wave motion is clear from the figures, with peak values of the SIF around $\omega a/c_S = 0.8$, around 1.0 for the EDIF and 1.1 for the MIIF. Fluctuations in the dynamic SIF and the EDIF of the magnetoelectroelastic composite exhibit a similar behavior to the previously observed for piezoelectric materials (Sáez et al., 2006). As expected, larger peak values of K_I are obtained with decreasing values of the angle branch β, while the opposite can be stated about K_{II}. Peak values of the EDIF K_{IV} are similar for the different branch angles. However, decreasing branch angles produce larger peak values of the MIIF K_V.

4.2. Circular arch crack

Scattering of L-waves by a curved circular arch crack is next considered. The geometry of the problem is shown in Fig. 5. Results are obtained for different values of the arch semi-angle α. The crack is meshed with eight discontinuous quadratic curved elements, plus 2 straight quarter-point elements at the tips with a small length of arch-length/30. The normalized field intensity factors at the crack tip are plotted against the dimensionless frequency in Fig. 10 (K_I), Fig. 11 (K_{II}), Fig. 12 (K_{IV}) and Fig. 13 (K_V).

As expected, peak values of the mode-I SIF decrease for increasing values of the arch angle α, whilst mode-II SIF follow the opposite tendency and increase with α for the considered plane wave excitation. This is due to the modification of the relative angle between the (tangent at the) crack tip and the incident motion.

To better illustrate the dynamic coupling effects, maps for both the vertical displacement (u_2/u_0) and the magnetic potential (φ/φ_0) amplitudes at two frequencies ($\omega a/c_S = 0.3,\ 0.8$) are included in

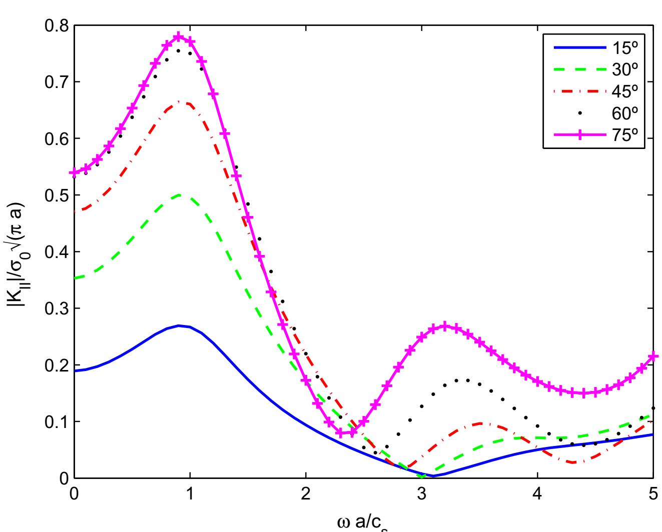

Fig. 11. L-wave scattering by a curved crack: K_{II} vs. frequency for different arch angles α.

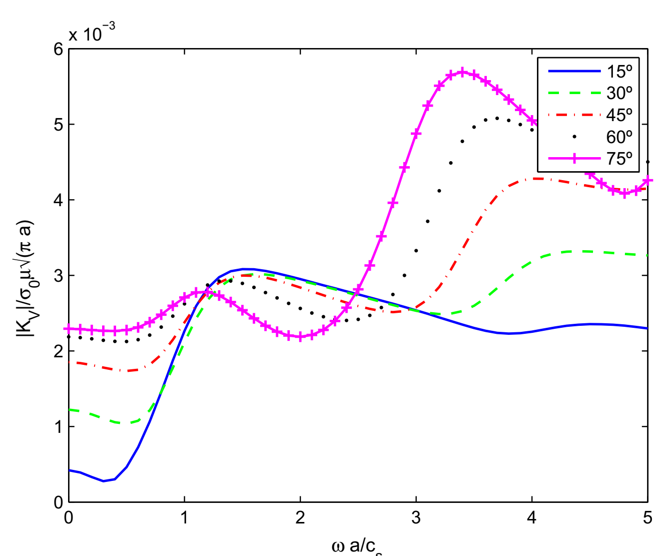

Fig. 13. L-wave scattering by a curved crack: K_V vs. frequency for different arch angles α.

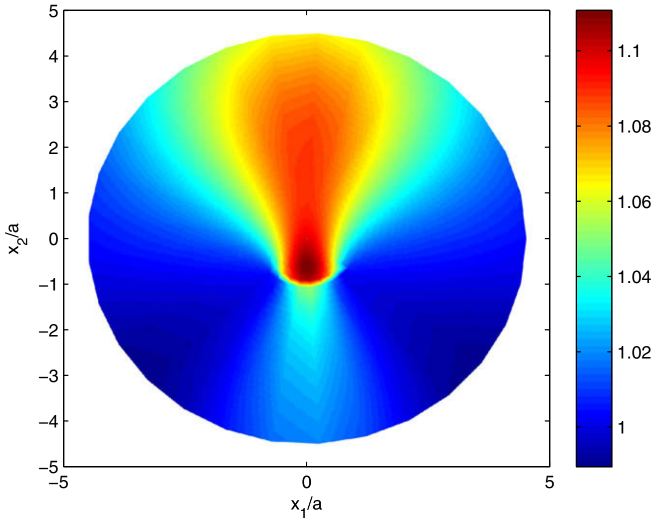

Fig. 14. L-wave scattering by a curved arch crack ($\alpha = 45$): vertical displacements amplitude u_2/u_0 at frequency $\omega a/c_S = 0.3$.

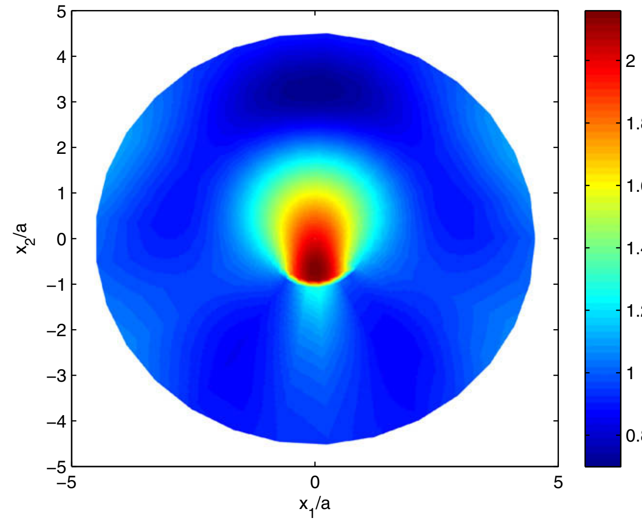

Fig. 16. L-wave scattering by a curved arch crack ($\alpha = 45$): vertical displacements amplitude u_2/u_0 at frequency $\omega a/c_S = 0.8$.

Figs. 14–17 for an arch semi-angle $\alpha = 45$. Those plots show amplitudes for total fields, i.e., incident plus scattered fields due to the presence of the crack.

5. Conclusions

This paper presents a time-harmonic BEM formulation for dynamic analysis of cracks in plane magnetoelectroelastic solids subjected to combined mechanical, magnetic and electric loadings. The formulation combines the classical displacement BIE and the hypersingular traction BIE. The fundamental solution derived by (Rojas-Diaz et al., 2008) using the Radon transform is implemented for the regular part, whilst an explicit static fundamental solution is implemented for the singular part (Jiang and Pan, 2004). In this way, strongly singular and hypersingular boundary integrals computation follows the previous work by the authors for static fracture analysis (García-Sánchez et al., 2007). Straight discontinuous quarter-point elements are used to capture the asymptotic behavior of the field variables near the crack tip and fracture parameter are directly extrapolated from the computed nodal values. Numerical results for the dynamic SIF, EDIF and MIIF are presented and discussed to demonstrate the accuracy and the efficiency of the present dynamic dual BEM.

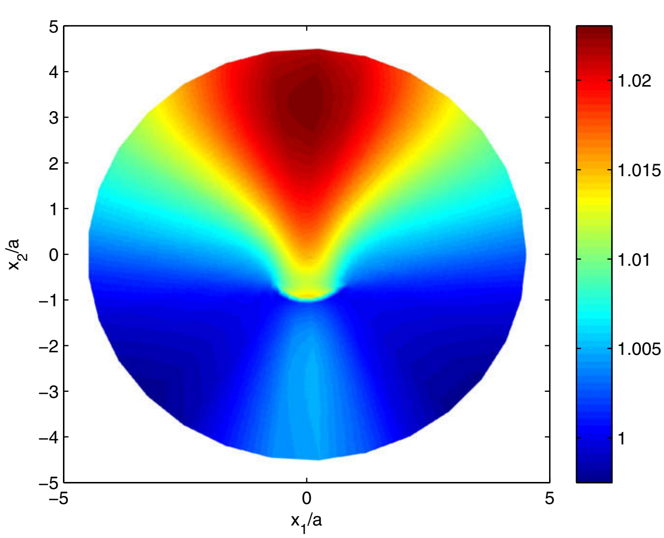

Fig. 15. L-wave scattering by a curved arch crack ($\alpha = 45$): magnetic potential amplitude φ/φ_0 at frequency $\omega a/c_S = 0.3$.

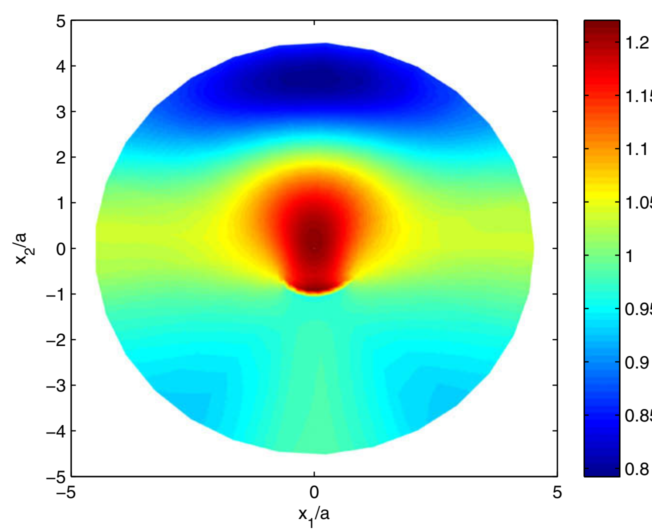

Fig. 17. L-wave scattering by a curved arch crack ($\alpha = 45$): magnetic potential amplitude φ/φ_0 at frequency $\omega a/c_S = 0.8$.

Acknowledgments

This work was supported by the *Ministerio de Ciencia e Innovación* of Spain and the *Consejería de Innovación, Ciencia y Empresa*of Andalucía (Spain) under projects*DPI2007-66792-C02-02* and *P06-TEP-02355*. The financial support is gratefully acknowledged.

Appendix A. Static fundamental solution in explicit form

For a 2D magnetoelectroelastic homogeneous solid, the displacement and traction at an observation point $\boldsymbol{x} = (x_1, x_2)$ in J-direction due to the application of an extended static point load at a source point $\boldsymbol{\xi} = (\xi_1, \xi_2)$ in I-direction can be written as (Jiang and Pan, 2004; Rojas-Diaz et al., 2008)

$$u^*_{IJ}(\boldsymbol{x}, \xi) = -\frac{1}{\pi}\Re[A_{JM}Q_{MI}\ln(z^x_M - z^\xi_M)] \tag{A.1}$$

$$p^*_{IJ}(\boldsymbol{x}, \xi) = \frac{1}{\pi}\Re\left[L_{JM}Q_{MI}\frac{\mu_M n_1 - n_2}{z^x_M - z^\xi_M}\right] \tag{A.2}$$

where z^x_M and z^ξ_M define the observation and source points location on the complex plane as

$$z^x_M = x_1 + \mu_M x_2; \quad z^\xi_M = \xi_1 + \mu_M\xi_2 \quad \text{with} \quad M = 1,2,4,5 \tag{A.3}$$

μ_M being the roots of the characteristic equation of the material with positive imaginary part. These roots and the columns of matrices $\mathbf{A}$ and $\mathbf{L}$ may be computed by solving the following eigenvalue problem

$$\left(\begin{array}{c|c} -\boldsymbol{T}^{-1}_{22}\boldsymbol{T}_{21} & -\boldsymbol{T}^{-1}_{22} \\ \hline -\boldsymbol{T}_{12}\boldsymbol{T}^{-1}_{22}\boldsymbol{T}_{21} + \boldsymbol{T}_{11} & -\boldsymbol{T}_{12}\boldsymbol{T}^{-1}_{22}\end{array}\right)\begin{pmatrix}\mathbf{A}_K \\ \mathbf{L}_K\end{pmatrix} = \mu_K\begin{pmatrix}\mathbf{A}_K \\ \mathbf{L}_K\end{pmatrix} \quad \text{(no sum on } K) \tag{A.4}$$

where

$$\boldsymbol{T}_{11} = C_{1IJ1}; \quad \boldsymbol{T}_{12} = C_{1IJ2}; \quad \boldsymbol{T}_{21} = C_{2IJ1}; \quad \boldsymbol{T}_{22} = C_{2IJ2}, \tag{A.5}$$

and matrix $\mathbf{Q}$ is obtained from

$$\mathbf{Q} = \mathbf{A}^{-1}\left[\mathbf{M}^{-1} + (\overline{\mathbf{M}})^{-1}\right]^{-1}; \quad \mathbf{M} = i\mathbf{A}\mathbf{L}^{-1} \tag{A.6}$$

where $\bar{\cdot}$ indicates complex conjugate.

Appendix B. Regularization of singular and hypersingular integrals

For the sake of completeness, a brief description of the integration procedure developed by the authors, García-Sánchez et al. (2005, 2006, 2007) and (Sáez et al., 2006), is next included.

After discretization of the boundaries and the field variables, integrals of the p^*, d^*-kernels of Eqs. (36) and (37), lead to basic singular integrals of kind

$$I_p = \int_{\Gamma_e}\frac{\mu_R n_1 - n_2}{z^x_R - z^\xi_R}\,\phi_q\,d\Gamma \quad \text{(no sum on } R), \tag{B.1}$$

$$I_d = \int_{\Gamma_e}\frac{\mu_R N_1 - N_2}{z^x_R - z^\xi_R}\,\phi_q\,d\Gamma \quad \text{(no sum on } R), \tag{B.2}$$

where ϕ_q are the boundary element shape functions, $\boldsymbol{n}$ is the outward normal at integration point and $\boldsymbol{N}$ is the outward normal at collocation points.

Both integrands in Eqs. (B.1) and (B.2) show strong singular behavior if the collocation point is in the integration element.

Similarly, integrals of the s^*-kernels lead to basic hypersingular integrals of type

$$I_s = \int_{\Gamma_e}\frac{\mu_R n_1 - n_2}{(z^x_R - z^\xi_R)^2}\,\phi_q\,d\Gamma \tag{B.3}$$

Considering the change of variables

$$\chi_R = z_R - z^\xi_R = (x_1 - \xi_1) + \mu_R(x_2 - \xi_2), \tag{B.4}$$

the Jacobian of the transformation that maps the boundary onto the complex plane has the expression

$$\frac{d\chi_R}{d\Gamma} = \frac{d\chi_R}{dx_1}\frac{dx_1}{d\Gamma} + \frac{d\chi_R}{dx_2}\frac{dx_2}{d\Gamma} = -n_2 + \mu_R n_1 \tag{B.5}$$

Taking into account Eqs. (B.4) and (B.5), I_p can be transformed to yield

$$I_p = \int_{\Gamma e}\frac{1}{\chi_R}\,\phi_q\,d\chi_R = \int_{\Gamma e}\frac{1}{\chi_R}\,(\phi - 1)\,d\chi_R + \int_{\Gamma e}\frac{1}{\chi_R}\,d\chi_R \tag{B.6}$$

where the first integral is regular and can be computed using a standard Gauss quadrature while the second one has a well known analytical solution.

Similarly, I_d can be transformed to yield

$$\begin{aligned} I_d &= \int_{\Gamma e}\frac{(\mu_R N_1 - N_2 \pm d\chi_R/d\Gamma)}{\chi_R}\,\phi_q\,d\Gamma \\ &= \int_{\Gamma e}\frac{(\mu_R N_1 - N_2 - d\chi_R/d\Gamma)}{\chi_R}\,\phi_q\,d\Gamma + \int_{\Gamma e}\frac{1}{\chi_R}\,\phi_q\,d\chi_R \end{aligned} \tag{B.7}$$

where the first of the integrals is regular since $d\chi_R/d\Gamma \to (\mu_R N_1 - N_2)$ as $\boldsymbol{x} \to \xi$. The second integral coincides with I_p and its computation has been described before.

Finally, I_s can be transformed with the help of Eqs. (B.4) and (B.5) as

$$I_s = \int_{\Gamma_e}\frac{1}{\chi^2_R}\,\phi\,d\chi_R \tag{B.8}$$

This integral is regularized by means of the Taylor series expansion of the shape function, ϕ_q, considered as a function of the complex χ_R variable, i.e.,

$$\begin{aligned} \phi(\chi_R \approx 0) &= \phi(\chi_R = 0) + \left.\frac{d\phi}{d\chi_R}\right|_{\chi_R=0}\chi_R + O(\chi^2_R) \\ &= \phi_0 + \phi'_0\chi_R + O(\chi^2_R) \end{aligned} \tag{B.9}$$

to yield

$$\begin{aligned} I_s &= \int_{\Gamma_e}\frac{1}{\chi^2_R}(\phi \pm (\phi_0 + \phi'_0\chi_R))d\chi_R \\ &= \int_{\Gamma_e}\frac{\phi - (\phi_0 + \phi'_0\chi_R)}{\chi^2_R}\,d\chi_R + \phi_0\int_{\Gamma_e}\frac{1}{\chi^2_R}\,d\chi_R \\ &\quad + \phi'_0\int_{\Gamma_e}\frac{1}{\chi_R}\,d\chi_R \end{aligned} \tag{B.10}$$

where the first integral is regular and the rest of integrals are singular and hypersingular, respectively, but having well known analytical solutions.

References

Eerenstein, W., Mathur, N.D., Scott, J.F., 2006. Multiferroic and magnetoelectric materials. Nature 442, 759–765.

Feng, W.J., Su, R.K.L., 2006. Dynamic internal crack problem of a functionally graded magneto-electro-elastic strip. Int. J. Solids Struct. 43, 5196–5216.

Feng, W.J., Pan, E., Wang, X., 2007. Dynamic fracture analysis of a penny-shaped crack in a magnetoelectroelastic layer. Int. J. Solids Struct. 44, 7955–7974.

Feng, W.J., Pan, E., 2008. Dynamic fracture behavior of an internal interfacial crack between two dissimilar magneto-electro-elastic plates. Eng. Fract. Mech. 75, 1468–1487.

Gao, C.F., Kessler, H., Balke, H., 2003a. Crack problems in magnetoelectroelastic solids. Part I: exact solution of a crack. Int. J. Eng. Sci. 41, 969–981.

Gao, C.F., Kessler, H., Balke, H., 2003b. Crack problems in magnetoelectroelastic solids. Part II: general solution of collinear cracks. Int. J. Eng. Sci. 41, 983–994.

Gao, C.F., Tong, P., Zhang, T.Y., 2004. Fracture mechanics for a mode III crack in a magnetoelectroelastic solid. Int. J. Solids Sturct. 41, 6613–6629.

García-Sánchez, F., Sáez, A., Domínguez, J., 2005. Anisotropic and piezoelectric materials fracture analysis by BEM. Comput. Struct. 83, 804–820.

García-Sánchez, F., Sáez, A., Domínguez, J., 2006. time-harmonic BEM for cracked anisotropic solids. Eng. Anal. Boundary Elem., 30 88–99.

García-Sánchez, F., Rojas-Díaz, R., Sáez, A., Zhang, Ch., 2007. Fracture of magnetoelectroelastic composite materials using boundary element method (BEM). Theor. Appl. Fract. Mech. 47, 192–204.

Hong, H., Chen, J.T., 1988. Derivations of integral equations of elasticity. J. Eng. Mech. ASCE 114, 1028–1044.

Hu, K., Li, G., 2005. Constant moving crack in a magnetoelectroelastic material under anti-plane shear loading. Int. J. Solids Struct. 42, 2823–2835.

Hu, K.Q., Kang, Y.L., Li, G.Q., 2006. Moving crack at the interface between two dissimilar magnetoelectroelastic materials. Acta Mech. 182, 1–16.

Jiang, X., Pan, E., 2004. Exact solution for 2D polygonal inclusion problem in anisotropic magnetoelectroelastic full-, half-, and bimaterial-planes. Int. J. Solids Struct. 41, 4361–4382.

Li, X.-F., 2005. Dynamic analysis of a cracked magnetoelectroelastic medium under antiplane mechanical and inplane electric and magnetic impacts. Int. J. Solids Struct. 42, 3185–3205.

Li, R., Kardomateas, G.A., 2006. The mode III interface crack in piezo-electro-magneto-elastic dissimilar bimaterials. ASME J. Appl. Mech. 73, 220–227.

Liang, J., 2008. The dynamic behavior of two parallel symmetric cracks in functionally graded piezoelectric/piezomagnetic materials. Arch. Appl. Mech. 78, 443–464.

Nan, C.W., 1994. Magnetoelectric effect in composite of piezoelectric and piezomagnetic phases, Phys. Rev. B 50, 6082–6088.

Parton, V.Z., Kudryavtsev, B.A., 1988. Electromagnetoelasticity. Gordon and Breach Science Publishers, New York.

Portela, A., Aliabadi, M.H., Rooke, D.P., 1992. The dual boundary element method: effective implementation for crack problems. Int. J. Numer. Meth. Eng. 33, 1269–1287.

Rojas-Diaz, R., Saez, A., García-Sánchez, F., Zhang, Ch., 2008. Time-harmonic Green's functions for anisotropic magnetoelectroelasticity. Int. J. Solids Struct. 45, 144–158.

Sáez, A., García-Sánchez, F., Domínguez, J., 2006. Hypersingular BEM for dynamic fracture in 2D piezoelectric solids. Comput. Methods Appl. Mech. Eng. 196, 235–246.

Shindo, Y., Ozawa, E., 1990. Dynamic analysis of a cracked piezoelectric material. In: Hsieh, R.K.T. (Ed.), Mechanical Modelling of New Electromagnetic Materials. Elsevier, pp. 297–304.

Sladek, J., Sladek, V., Solek, P., Pan, E., 2008. Fracture analysis of cracks in magneto-electro-elastic solids by the MLPG. Comput. Mech. 42, 697–714.

Soh, A.K., Liu, J.X., 2005. On the constitutive equations of magnetoelectroelastic solids. J. Intell. Mater. Syst. Struct. 16, 597–602.

Su, R.K.L., Feng, W.J., Liu, J., 2007. Transient response of interface cracks between dissimilar magneto-electro-elastic strips under out-of-plane mechanical and in-plane magneto-electrical impact loads. Compos. Struct. 78, 119–128.

Tian, W.Y., Gabbert, U., 2004. Multiple crack interaction problem in magnetoelectroelastic solids. Eur. J. Mech. A/Solids 23, 599–614.

Tian, W.Y., Rajapakse, R.K.N.D., 2005. Fracture analysis of magnetoelectroelastic solids by using path independent integrals. Int. J. Fract. 131, 311–335.

Van Suchtelen, J., 1972. Product properties: a new application of composite materials. Phillips Research Reports. 27, 28–37.

Voigt, W., 1910. Lehrbuch der Kristallphysik. B.G. Teubner, Leipzig.

Wang, B.L., Mai, Y.W., 2003. Crack tip field in piezoelectric/piezomagnetic media. Eur. J. Mech. A/Solids 22, 591–602.

Wang, B.L., Mai, Y.W., 2004. Fracture of piezoelectromagnetic materials. Mech. Res. Commun. 31, 65–73.

Wang, B.L., Mai, Y.W., 2007. Applicability of the crack-face electromagnetic boundary conditions for fracture of magnetoelectroelastic materials. Int. J. Solids Struct. 44, 387–398.

Yong, H.-d., Zhou, Y.-h., 2007. Transient response of a cracked magnetoelectroelastic strip under anti-plane impact. Int. J. Solids Struct. 44, 705–717.

Zhang, P.-W., Zhou, Z.-G., Wang, B., 2007. Dynamic behavior of two collinear interface cracks between two dissimilar functionally graded piezoelectric/piezomagnetic material strips. Appl. Math. Mech. 28, 615–625.

Zhong, X.-C., Li, X.-F., 2006. A finite length crack propagating along the interface of two dissimilar magnetoelectroelastic materials. Int. J. Eng. Sci. 44, 1394–1407.

Zhou, Z.-G., Wang, B., 2005. Scattering of harmonic anti-plane shear waves by an interface crack in magneto-electro-elastic composites. Appl. Math. Mech. 26, 17–26.

Zhou, Z.-G., Wu, L.-Z., Wang, B., 2005. The dynamic behavior of two collinear interface cracks in magneto-electro-elastic materials. Eur. J. Mech., A/Solids 24, 253–262.

Zhou, Z.-G., Wang, B., 2006. Dynamic behavior of two parallel symmetry cracks in magneto-electro-elastic composites under harmonic anti-plane waves. Appl. Math. Mech. 27, 583–591.

Zhou, Z.-G., Wu, L.-Z., Du, S.-Y., 2006. The dynamic behavior of two parallel interface cracks in magneto-electro-elastic materials under the harmonic anti-plane shear stress waves. Strength Fract. Complexity 4, 169–184.

Zhou, Z.-G., Wang, B., 2008. An interface crack between two dissimilar functionally graded piezoelectric/piezomagnetic material half infinite planes subjected to the harmonic anti-plane shear stress waves. Int. J. Appl. Electromagn. Mech. 27, 117–132.